Magnetism, Magnetotransport and Magnetic Structure of $ThCu_3Mn_4O_{12}$, Prepared at Moderate Pressures

Javier Sánchez-Benítez[a], María J. Martínez-Lope[b], and José A. Alonso[b]

[a] Centre for Science at Extreme Conditions and School of Engineering and Electronics,
University of Edinburgh, King's Buildings, Mayfield Road, Edinburgh EH9 3JZ, UK
[b] Instituto de Ciencia de Materiales de Madrid, CSIC, Cantoblanco, E-28049 Madrid, Spain

Reprint requests to Prof. Dr. J. A. Alonso. E-mail: ja.alonso@icmm.csic.es

Dedicated to Professor Gérard Demazeau on the occasion of his 65th birthday

The complex perovskite $ThCu_3Mn_4O_{12}$ has been prepared at moderate pressures of 2 GPa. With respect to the parent compound $CaCu_3Mn_4O_{12}$, the replacement of Ca^{2+} by Th^{4+} involves a double electronic injection that leads to a substantial increment of T_C, up to 370 K. The crystal structure was refined in the space group $Im\bar{3}$ from NPD data collected with $\lambda = 1.33$ Å at r. t. An additional NPD pattern recorded at 1.8 K with $\lambda = 2.42$ Å allowed to refine the magnetic structure, which displays a ferrimagnetic coupling between Mn^{3+}/Mn^{4+} and Cu^{2+} spins, aligned along the c direction. The refined magnetic moments at the Mn and Cu substructures of 2.5 and -0.5 μ_B, respectively, account for the observed saturation magnetisation at 2 K, of 7 μ_B/f. u. A semiconducting behaviour is observed between 10 and 350 K which can be correlated with the appearance of a gap in the conduction band for the $\sim$50 % Mn^{3+}/50 % Mn^{4+} mixed valence observed in the B substructure of this perovskite.

Key words: Perovskite Oxide, Colossal Magnetoresistance, Ferrimagnetic Oxide, Neutron Powder Diffraction, Mn Mixed Valence, High-pressure Synthesis

Introduction

The discovery of "colossal" magnetoresistance (CMR) in $La_{1-x}Sr_xMnO_3$-type compounds [1, 2] together with its many unusual properties has attracted considerable attention. Very few oxide systems have been described to show these appealing properties, simultaneously exhibiting ferromagnetic and half-metallic character [3]. Besides the simple oxides CrO_2 and Fe_3O_4, some selected complex oxides such as the pyrochlore $Tl_2Mn_2O_7$ or the double perovskite Sr_2FeMoO_6 have been demonstrated to show non-negligible MR at r. t., as required for technological applications [4]. The colossal magnetoresistance phenomenon is an interesting physical bearing that can appear in materials where some degrees of freedom are simultaneously active [5]. The electronic complexity of these compounds, showing charge, spin, but also lattice and orbital degrees of freedom, leads to giant responses to small perturbations [6].

Among these few half-metallic oxides, the complex perovskite $CaCu_3Mn_4O_{12}$ [7, 8] has attracted the interest of solid-state scientists since it exhibits a considerable low-field magnetoresistance at r. t., decoupled with T_C (355 K). The crystal structure of $CaCu_3Mn_4O_{12}$ [9] has the particularity of containing Cu^{2+} (or other Jahn-Teller transition metal cations, such as Mn^{3+}) at the A positions of the ABO_3 perovskite, ordered together with Ca^{2+} in a $2a_0 \times 2a_0 \times 2a_0$ cubic cell of body-centred symmetry ($a_0 =$ unit cell of the perovskite aristotype). Given the small size of the A cations, there is an important tilting of the MnO_6 octahedra, providing an effective square-planar coordination for Cu^{2+}, whereas Ca^{2+} is located in a perfectly regular 12-fold coordinated oxygen environment.

This structural type has been demonstrated to be able to accommodate a large variety of chemical substitutions, either at the Ca, Cu or Mn substructures [10] in the family of general stoichiometry $A'A_3B_4O_{12}$. For instance, the replacement of Ca^{2+} cations by rare earths in the $ECu_3Mn_4O_{12}$ ($E =$ rare earths) family, implies an electron doping effect that affects the magnetic and transport properties, as demonstrated recently [11, 12]. Whereas the synthesis of many materials of the $A'A_3B_4O_{12}$ family has been described to

require high-pressure conditions (7 GPa), necessary to stabilise the small *A* cations in the twelve-fold positions of the perovskite, recently, we have been able to synthesise some new derivatives of CaCu$_3$Mn$_4$O$_{12}$ at moderate pressures of 2 GPa, starting with very reactive precursors, obtained by wet-chemistry techniques [13]. The electron injection can be doubled in materials where Ca is replaced by a tetravalent cation with suitable size, typically Th^{4+} or Ce^{4+}. In this work, we present magnetic and magnetotransport results on ThCu$_3$Mn$_4$O$_{12}$, prepared at 2 GPa starting from citrate precursors; the crystal and magnetic structure were also studied from NPD data, confirming previous reports regarding the ferrimagnetic coupling of Mn and Cu substructures [14].

Experimental Section

ThCu$_3$Mn$_4$O$_{12}$ was obtained as a black polycrystalline powder by a chemical route using citrates as precursors. Stoichiometric amounts of analytical grade Th(NO$_3$)$_4$·5H$_2$O, Cu(NO$_3$)$_2$·3H$_2$O and MnCO$_3$ were dissolved in citric acid. The solution was slowly evaporated, leading to a resin which was dried at 120 °C. The sample was then heated at 600 °C for 12 h in order to eliminate all the organic materials and nitrates. This precursor was thoroughly ground with KClO$_4$ (30 % in weight), put into a gold capsule (8 mm diameter, 10 mm length), sealed, and placed in a cylindrical graphite heater. The reaction was carried out in a piston-cylinder press (Rockland Research Co.) at a hydrostatic pressure of 2 GPa at 1000 °C for 60 min. Then the material was quenched to r. t., and the pressure was subsequently released. The "*in situ*" decomposition of KClO$_4$ provides the high O$_2$ pressure required to stabilise Mn^{4+} cations. A fraction of the raw product, obtained as a dense, homogeneous pellet, was partially ground to perform the structural and magnetic characterisation; some as-grown pellets were kept for magnetotransport measurements. The ground product was washed in a dilute HNO$_3$ aqueous solution, in order to dissolve KCl coming from the decomposition of KClO$_4$ and to eliminate small amounts of unreacted CuO; then the powder sample was dried in air at 150 °C for 1 h.

The characterisation by XRD was performed using a Bruker-AXS D8 diffractometer (40 kV, 30 mA), controlled by the Diffract^{plus} software, in Bragg-Brentano reflection geometry with CuK_α radiation (λ = 1.5418 Å). A secondary graphite monochromator allowed the complete removal of CuK_β radiation. The data were obtained between 10 and 100° 2θ in steps of 0.05°. Neutron powder diffraction (NPD) patterns were acquired at the high-flux D20 diffractometer of the Institut Laue-Langevin in Grenoble. The sample, weighing 1 g, was packed in a vanadium holder of 6 mm diameter. A pattern was collected at r. t. with a wavelength of

1.33 Å and a counting time of 30 min in the high-resolution mode, with 10′ collimation. A low-temperature (1.8 K) diagram was recorded with a wavelenght of 2.42 Å for 30 min in order to investigate the magnetic structure. The NPD patterns were analysed by Rietveld methods, using the program Fullprof [15]. The line shape of the diffraction peaks was generated by a pseudo-Voigt function and the background refined to a 5th-degree polynomial. The coherent scattering lengths for Th, Cu, Mn, and O were, respectively, 10.31, 7.718, −3.73 and 5.803 fm. In the final run the following parameters were refined: background coefficients, zero-point, half-width, pseudo-Voigt and asymmetry parameters for the peak shape; scale factor, positional, occupancy factors for oxygens, isotropic displacement factors for all the atoms and the unit cell parameters.

The *dc* magnetic susceptibility was measured with a commercial SQUID magnetometer on powdered samples in the temperature range 5 – 400 K with an applied field of 0.1 T; magnetisation isotherms were recorded at 2, 150, 300 and 370 K between −5 T and +5 T; transport and magnetotransport measurements were performed by the conventional four-probe technique, under magnetic fields up to 9 T in a PPMS system from Quantum Design.

Results and Discussion

ThCu$_3$Mn$_4$O$_{12}$ oxide was obtained as a well-crystallised powder. The laboratory XRD diagram is characteristic of a cubic perovskite showing sharp, well-defined superstructure reflections due to the 1 : 3 ordering of Th and Cu cations, and can all be indexed in the space group $Im\bar{3}$. The unit cell parameter is a = 7.4058(5) Å. This is much superior to the unit cell dimension of the parent compound CaCu$_3$Mn$_4$O$_{12}$ (a = 7.241 Å [9]) due to the double injection of electrons realised when replacing Ca^{2+} by Th^{4+}.

Structural refinement

The structural refinement of ThCu$_3$Mn$_4$O$_{12}$ was performed from r. t. NPD data in the space group $Im\bar{3}$ (no. 204), using the CaCu$_3$Mn$_4$O$_{12}$ structure as starting model [9], with Th atoms at 2a (0, 0, 0), Cu at 6b (0, 1/2, 1/2), Mn at 8c (1/4, 1/4, 1/4) and O at 24g (x, y, 0) sites. A reasonable fit ($R_I \approx 6$ %) was obtained for this preliminary model. As a second step, the possibility that some Mn^{3+} cations occupy some of the Cu^{2+} positions at 6b sites was considered, and the complementary occupancy factors were refined, constrained to full occupancy. Neutron diffraction is specially suited to detect a small fraction of Mn at Cu positions, given the contrasting scattering lengths for both elements. After

Table 1. Structural parameters for $ThCu_3Mn_4O_{12}$ refined in the cubic space group $Im\bar{3}$ at r. t. from NPD data[a].

Atom	W.-site	x	y	z	f_{occ}	B (Å²)
Th	2a	0	0	0	1.0	−0.1(1)
Cu	6b	0	1/2	1/2	0.952(8)	0.13(7)
Mn	6b	0	1/2	1/2	0.048(8)	0.13(7)
Mn	8c	1/4	1/4	1/4	1.0	1.8(1)
O	24g	0.2994(4)	0.1758(3)	0	1.0	0.32(4)

[a] Lattice parameters: $a = 7.4058(5)$ Å, $V = 406.18(5)$ Å³; discrepancy factors: $R_P = 3.32\%$, $R_{wp} = 4.45\%$, $R_{exp} = 0.70\%$, $\chi^2 = 39.2$ and $R_{Bragg} = 4.88\%$.
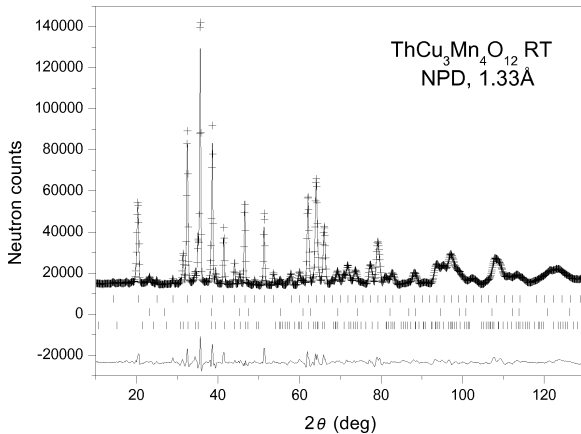
Table 2. Main bond lengths (Å) and selected angles (deg) for $ThCu_3Mn_4O_{12}$ determined from NPD data at r. t.

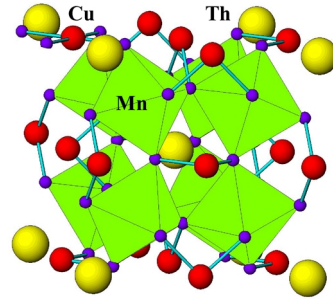| Th–O (×12)	2.571(2)		
CuO₁₂ polyhedra		*MnO₆ octahedra*	
Cu–O (×4)	1.976(2)	Mn–O (×6)	1.966(2)
Cu–O (×4)	2.823(1)	O–Mn–O	92.1(1)
Cu–O (×4)	3.268(2)	O–Mn–O	87.9(1)
O–Cu–O	97.5(2)	Cu–O–Mn	108.91(8)
O–Cu–O	82.5(2)	Mn–O–Mn	140.77(4)

Fig. 2. View of the crystal structure of $ThCu_3Mn_4O_{12}$ (*c* axis vertical; *a* axis from right to left). Corner-sharing $(Mn)O_6$ octahedra are tilted in the structure to optimise Th–O and Cu–O bond lengths; the square-planar coordination of Cu is highlighted.

Fig. 1. Observed (crosses), calculated (full line) and difference (bottom) NPD Rietveld profiles for $ThCu_3Mn_4O_{12}$ at r. t., collected at the high-flux D20-ILL diffractometer. The second and third series of tick labels correspond to the minor ThO_2 and $K_2Mn_8O_{16}$ (hollandite) impurities.

this refinement the quality of the fit was slightly improved, reaching a discrepancy factor of $R_I = 4.88\%$. The subsequent refinement of the occupancy factor for oxygen positions confirmed the full stoichiometry of the oxygen substructure. The presence of two impurity phases, ThO_2 and $K_2Mn_8O_{16}$ with hollandite structure (coming from a collateral reaction with $KClO_4$) was considered by including their crystal structures as second and third phases in the refinement (Fig. 1). The final crystallographic formula for the main perovskite phase resulted to be $Th[Cu_{2.86(2)}Mn_{0.14(2)}]_{6b} [Mn_4]_{8c} O_{11.6(1)}$, with 6b/8c being the respective Wyckoff sites occupied. Assuming a valence of 2+ for Cu cations, 3+ for Mn at the 6b substructure, and 4+ for Th, the nominal valence for Mn at 8c positions is 3.47(2)+. This average value corresponds to 47% Mn^{4+} and 53% Mn^{3+}. From the present NPD data there is no sign of long-range ordering between Mn^{4+} and Mn^{3+}, which are distributed at random over the *B* positions of the perovskite. Table 1 includes the main atomic pa-

rameters and discrepancy factors after the refinement. Fig. 1 shows the good agreement between the observed and calculated NPD profiles at r. t. Table 2 contains a list of selected bond lengths and angles.

The cubic perovskite superstructure of $ThCu_3Mn_4 O_{12}$ is represented in Fig. 2, and contains several features that must be highlighted. The Th atoms are coordinated to 12 oxygen atoms, with equal Th–O distances of 2.57 Å, while the oxygen environment for the Cu^{2+} cations is highly irregular, with 8 rather long distances (2.82 and 3.27 Å at r. t.) and an effective coordination number of four, with Cu–O bond lengths of 1.976 Å in a pseudo-square arrangement (Table 2). These CuO_4 units are not strictly square, exhibiting O–Cu–O angles of 97.5 and 82.5°. At the *B* substructure of the perovskite, (Mn^{4+}, Mn^{3+}) cations occupy the centres of virtually regular octahedra, with Mn–O bond lengths of 1.966(2) Å at r. t. This distance is significantly longer than that observed for $CaCu_3Mn_4O_{12}$, of 1.915(1) Å [9] consistent with the incorporation of the larger Mn^{3+} cations in the Mn^{4+} substructure as a consequence of the electron doping effect. As shown in Fig. 2, the perovskite structure is fairly distorted due to the small size of the Th^{4+} and Cu^{2+} cations, which force the MnO_6 octahedra to tilt in order to optimise the Th–O and Cu–O bond lengths. The tilt-

ing angle of the octahedra can simply be derived from the Mn–O–Mn angle (140.8°), to be 19.6° at r. t. It is remarkable that, despite the increase in size of the MnO$_6$ octahedra with respect to the undoped compound, which would suggest a decrease of the tolerance factor of the perovskite structure and, hence, an increment of the tilting effect of the octahedra, we observe a virtually unchanged Mn–O–Mn angle (142° for CaCu$_3$Mn$_4$O$_{12}$ [9]). In this peculiar superstructure of perovskite, the tilting angle of the octahedra is strongly determined by the CuO$_4$ square-planar units in such a way that an increase in the octahedral size is accommodated by an expansion of the ThO$_{12}$ and CuO$_4$ units, which are, in this case, under a certain tensile stress.

Magnetic properties

The magnetic susceptibility *vs.* temperature curve shown in Fig. 3 exhibits the abrupt increase characteristic of a spontaneous ferrimagnetic ordering. The spontaneous magnetisation corresponds to the opposite alignment of Cu$_{6b}$ and Mn$_{8c}$ magnetic moments. The Curie temperature of 370 K is considerably higher than that observed for the undoped ferrimagnetic system Ca(Cu$_{2.5}$Mn$_{0.5}$)Mn$_4$O$_{12}$ (T_C = 345 K) [16]. The magnetisation *vs.* magnetic field isotherms (Fig. 4a) collected at T = 2, 150, 300 and 370 K are also characteristic of a ferromagnetic ordering, exhibiting a maximum saturation magnetisation of 7.2 μ_B/f. u. at 2 K. The coercive fields of the hysteresis cycles decrease linearly as temperature increases, as shown in Fig. 4b. The saturation magnetisation observed at 2 K is very much reduced with respect to that expected for a perfect ferrimagnetic structure of (Mn$^{3+}_2$Mn$^{4+}_2$)
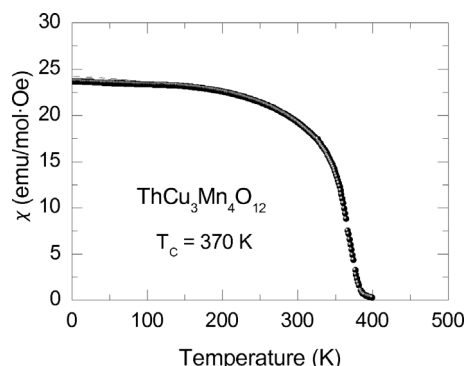

Fig. 3. Temperature dependence of the *dc* magnetic susceptibility. The dotted line corresponds to the expected magnetisation following the $T^{3/2}$ dependence dictated by the Block law.
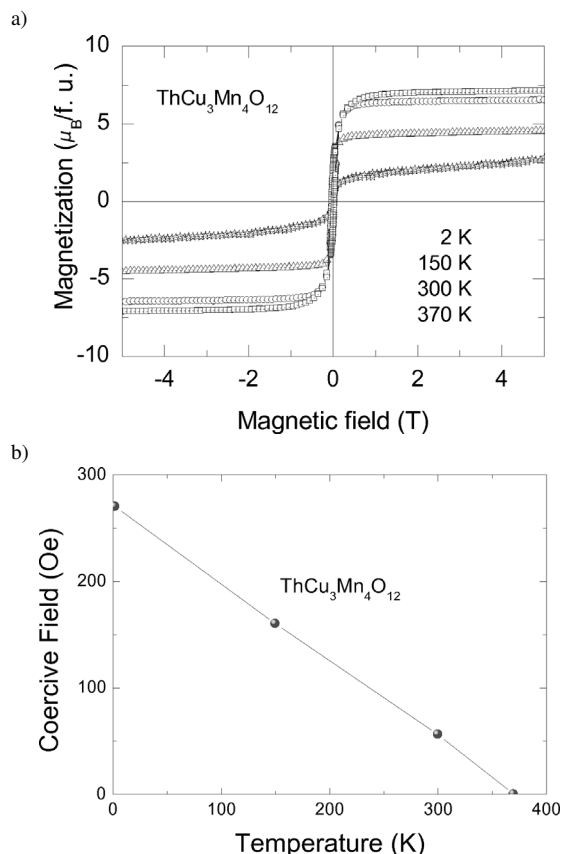

Fig. 4. Magnetisation isotherms at T = 2, 150, 300 and 370 K.

and (Cu$^{2+}_3$) spins, of 11 μ_B/f. u. The Goodenough-Kanamori rules predict a ferromagnetic coupling for Mn^{4+}–O–Mn^{4+} pairs with superexchange angles close to 90°, but the superexchange is antiferromagnetic (AFM) across Mn^{4+}–O–Mn^{3+} paths. For the ~50 % Mn^{3+}/50 % Mn^{4+} present in the B substructure of this oxide there may be a large rate of AFM coupling, which undoubtedly would decrease the saturation magnetisation, as observed. The absence of long-range ordering between Mn^{3+} and Mn^{4+} cations at the B substructure would give rise to a considerable magnetic frustration, preventing the development of a full long-range magnetic ordering.

Magnetic structure

On the low-temperature NPD diagram collected at 1.8 K with λ = 2.42 Å there is evidence for a magnetic contribution to the scattering on the low-angle Bragg reflections, particularly visible on the [2 2 0] Bragg position, at $2\theta \approx 55.6°$. This contribution is characteristic
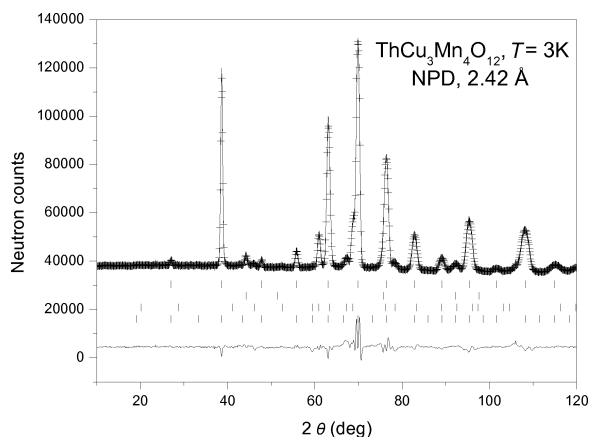
Fig. 5. Observed (crosses), calculated (full line) and difference (bottom) NPD Rietveld profiles for $ThCu_3Mn_4O_{12}$ at 1.8 K. The second and third series of tick labels correspond to the minor ThO_2 and $K_2Mn_8O_{16}$ (hollandite) impurities, the fourth series correspond to the magnetic structure.

of a ferromagnetic ordering, in which the magnetically ordered unit cell coincides with the crystallographic one. We have modeled a collinear ferrimagnetic structure, implying an antiferromagnetic coupling of the Mn and Cu magnetic moments, as it has been suggested from band-structure calculations [17] for the parent $CaCu_3Mn_4O_{12}$ compound. We have modeled a perfect ferrimagnetic ordering between the magnetic moments at $8c$ and $6b$ positions and refined this model for the 1.8 K NPD data. After the full refinement of the profile, including the magnetic moments, a discrepancy factor R_{mag} of 8.2 % was reached. The refinement led to ordered moments of 2.24(9) μ_B and $-0.47(11)$ μ_B for the $8c$ and $6b$ sites, respectively, oriented along the [001] direction. Both values are noticeably reduced from those expected for a random distribution of Mn^{3+}/Mn^{4+} over the $8c$ sites, of 3.5 μ_B per site, and from Cu^{2+} (with less than 5 % of Mn^{3+} at the $6c$ sites) of ~ -1 μ_B. From the refined ordered magnetic moments at both sublattices we can estimate a saturation magnetisation of 7.55 μ_B/f. u., which is in excellent agreement with the experimental value (7.2 μ_B/f. u.). Fig. 5 displays the goodness of the fit to the experimental NPD profile after the Rietveld refinement of the magnetic structure. It is also important to underline that the crystal structure at 1.8 K, refined together with the magnetic structure, does not show any superstructure reflection which could indicate the presence of long-range ordering (charge ordering) of Mn^{3+}/Mn^{4+} at the B substructure of the perovskite.
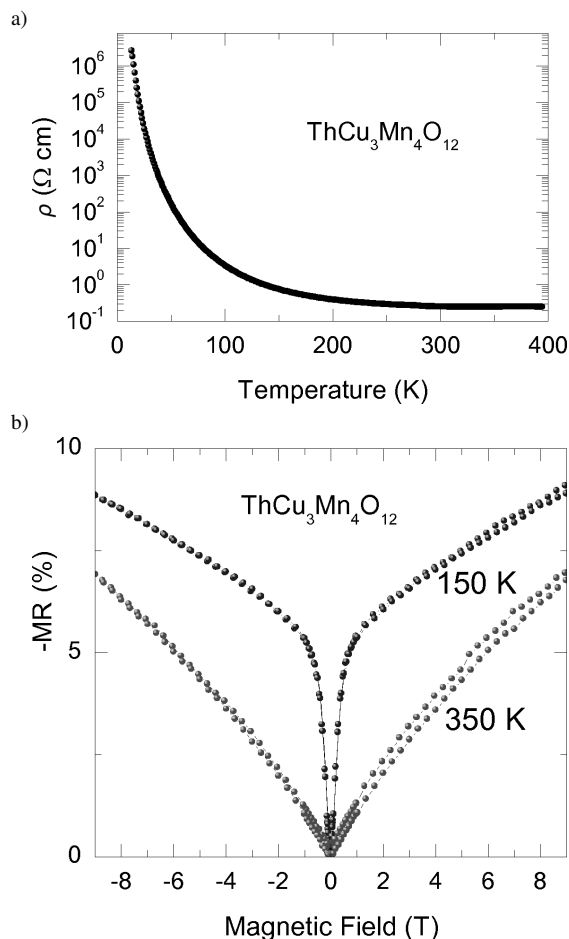

Fig. 6. a) Resistivity *vs.* temperature and b) magnetoresistance isotherms at 150 and 350 K. MR is defined as $100 \times [R(9T)–R(0)]/R(0)$.

The pattern can be correctly fitted within the symmetry of the space group $Im\bar{3}$.

Electrical properties

Fig. 6a shows the resistivity *vs.* temperature plot, characteristic of a semiconducting behaviour, with a value for $\rho(T = 300$ K$)$ of around 0.26 $\Omega \cdot$ cm, which is considerably lower than that described for the parent $CaCu_3Mn_4O_{12}$ compound ($\sim 1.8 \times 10^3$ Ω cm [7]). This low resistivity value suggests an increase of the carrier density with respect to the parent compound, probably related to the mixed-valence state induced on the Mn cations at the B positions of the perovskite as a consequence of the replacement of Ca^{2+} by Th^{4+}. Nevertheless, it is surprising that thermally activated

semiconducting behaviour is observed in this sample, in contrast with the metallic behaviour observed for many members of the ECu$_3$Mn$_4$O$_{12}$ series with E = trivalent rare earths. Taking into account that the amount of Mn^{3+} and Mn^{4+} at the B sites is virtually 50 %, we hypothesise that, as it frequently happens in transition metal oxides with a half-filled conduction band, there is a gap opening in this band giving rise to the observed insulating or semiconducting behaviour [18]. In any case, the observed insulating behaviour is not comparable to that of a standard semiconductor. Its resistivity is thermally activated but it does neither follow a simple law $R = R_0 \exp(Ea/k_B T)$, nor any other standard regime of conductivity *via* polarons.

Regarding the changes in resistance under a magnetic field we define MR(H) = $100 \times$ [R(H)–R(0)]/R(0). Fig. 6b illustrates the evolution of MR *vs.* the magnetic field as isotherms at 150 and 350 K in the range $H = 0 - 9$ T for ThCuMn$_4$O$_{12}$. The magnetoresistance increases with decreasing temperature, reaching a maximum value of -9.0 % at 150 K and 9 T. At 350 K there is a non-negligible magnetoresistance of -6.9 % at 9 T. The most striking feature of these isotherms is the strong component of low-field MR, defined for magnetic fields lower than 1 T. A value of MR (1 T) higher than 5.5 % is observed at 150 K, and it is not negligible (about 1 %) at r. t. These figures make this compound a candidate for applications in spintronic devices.

Conclusions

The complex perovskite ThCu$_3$Mn$_4$O$_{12}$ has been synthesised at a moderate pressure of 2 GPa in the presence of an oxidising agent. The structural refinement from NPD data at r. t. shows that the 6b positions of the perovskite are randomly occupied by Cu^{2+} and 5 % Mn^{3+} cations; the magnetic structure corresponds to an antiferromagnetic arrangement of Cu$^{2+}_{6b}$ and (Mn^{3+},Mn^{4+})$_{8c}$, giving rise to a global ferrimagnetic structure. The tilting angle of the MnO$_6$ octahedra does not significantly evolve from the parent CaCu$_3$Mn$_4$O$_{12}$ compound, in spite of the expansion of the octahedral units, since the tilting is strongly determined by the almost square-planar CuO$_4$ units. The ferromagnetic T_C is considerably enhanced (T_C = 370 K) with respect to the Ca compound (T_C = 345 K) due to the double electron injection realised upon replacing Ca^{2+} by Th^{4+}. Despite the 50 % Mn^{4+}/50 % Mn^{3+} ratio observed at the B positions of the perovskite, there is no sign of charge ordering either at r. t. or 1.8 K. The resistivity shows a thermally activated behaviour which could be due to the opening of a gap in the conduction band for this particular Mn^{4+}/Mn^{3+} ratio; the low-field MR at r. t. is substantial (1 % at 1 T) and could be exploited in spintronic devices.

[1] R. von Helmholt, J. Wecker, B. Holzapfel, L. Schultz, K. Samwer, *Phys. Rev. Lett.* **1993**, *71*, 2331.

[2] Y. Tokura, *Colossal Magnetoresistance Oxides*, Gordon and Breach, London **2000**.

[3] A. P. Ramirez, *J. Phys: Condens. Matter* **1997**, *9*, 8171.

[4] M. Ziese, *Rep. Prog. Phys.* **2002**, *65* 143.

[5] E. Dagotto, T. Hotta, A. Moreo, *Phys. Rep.* **2001**, *344*, 1.

[6] E. Dagotto, *Science* **2005**, *309*, 258.

[7] Z. Zeng, M. Greenblatt, M. A. Subramanian, M. Croft, *Phys. Rev. Lett.* **1999**, *82* 3164.

[8] Z. Zeng, M. Greenblatt, J. E. Sunstrom, M. Croft, S. Khalid, *J. Sol. State Chem.* **147** 185 (1999).

[9] J. Chenavas, J. C. Joubert, M. Marezio, B. Bochu, *J. Solid State Chem.* **1975**, *14*, 5.

[10] M. A. Subramanian, A. W. Sleight, *Solid State Sci.* **2002**, *4*, 347.

[11] J. A. Alonso, J. Sánchez-Benítez, A. de Andrés, M. J. Martínez-Lope, M. T. Casais, J. L. Martínez, *Appl. Phys. Lett.* **2003**, *83*, 2623.

[12] J. Sánchez-Benítez, J. A. Alonso, A. de Andrés, M. J. Martínez-Lope, M. T. Casais, J. L. Martínez, *J. Magn. Magn. Mater.* **2004**, *272*, 1407.

[13] J. Sánchez-Benítez, J. A. Alonso, H. Falcón, M. J. Martínez-Lope, A. de Andrés, M. T. Fernández-Díaz, *J. Phys.: Condens. Matter* **2005**, *17*, S30 – 63.

[14] A. Collomb, D. Samaras, G. Fillion, M. N. Deschizeaux, J. C. Joubert, *J. Magn. Magn. Mater.* **1978**, *8*, 77.

[15] J. Rodríguez-Carvajal, *Physica B* **1993**, *192*, 55.

[16] J. Sánchez-Benítez, J. A. Alonso, M. J. Martínez-Lope, M. T. Casais, J. L. Martínez, A. de Andrés, M. T. Fernández-Díaz, *Chem. Mater.* **2003**,*15*, 2193.

[17] R. Weht, W. E. Pickett, *Phys. Rev. B* **2001**, *65*, 14415.

[18] J. Sánchez-Benítez, A. de Andrés, M. García Hernández, J. A. Alonso, M. J. Martínez-Lope, *Mater. Sci. Eng. B* **2006**, *126*, 262.